The Journal of Chemical Physics

Applicability of multipole decomposition to plasmonic- and dielectric-lattice resonances

Cite as: J. Chem. Phys. **156**, 114104 (2022); https://doi.org/10.1063/5.0082005
Submitted: 11 December 2021 • Accepted: 21 February 2022 • Accepted Manuscript Online: 22 February 2022 • Published Online: 15 March 2022

Aoxue Han, Jerome V. Moloney and Viktoriia E. Babicheva

The Journal of Chemical Physics ARTICLE scitation.org/journal/jcp

Applicability of multipole decomposition to plasmonic- and dielectric-lattice resonances

Cite as: J. Chem. Phys. 156, 114104 (2022); doi: 10.1063/5.0082005
Submitted: 11 December 2021 • Accepted: 21 February 2022 •
Published Online: 15 March 2022

Aoxue Han,[1,a] Jerome V. Moloney,[1,a] and Viktoriia E. Babicheva[2,b]

AFFILIATIONS

[1] James C. Wyant College of Optical Sciences, University of Arizona, Tucson, Arizona 85721, USA
[2] Department of Electrical and Computer Engineering, University of New Mexico, Albuquerque, New Mexico 87131, USA

Note: This paper is part of the JCP Special Topic on Advances in Modeling Plasmonic Systems.
[a] **Also at:** Arizona Center for Mathematical Sciences, University of Arizona, Tucson, Arizona 85721, USA.
[b] **Author to whom correspondence should be addressed:** vbb@unm.edu

ABSTRACT

Periodic nanoparticle arrays have attracted considerable interest recently since the lattice effect can lead to spectrally narrow resonances and tune the resonance position in a broad range. Multipole decomposition is widely used to analyze the role of the multipoles in the resonance excitations, radiation, and scattering of electromagnetic waves. However, previous studies have not addressed the validity and accuracy of the multipole decomposition around the lattice resonance. The applicability of the exact multipole decomposition based on spherical harmonics expansion has not been demonstrated around the lattice resonance with the strong multipole coupling. This work studies the two-dimensional periodic arrays of both plasmonic and dielectric nanospheres and compares the multipole decomposition results with the analytic ones around their lattice resonances. We study both the effective polarizabilities of multipoles and the scattering spectra of the structures. The analytical results are calculated from the coupled dipole–quadrupole model. This study demonstrates that the exact multipole decomposition agrees well with the numerical simulation around lattice resonances. Only a small number of multipoles are required to represent the results accurately.

I. INTRODUCTION

Recently, metasurfaces have attracted much interest due to their great potential in optical applications, photonics, sensing, and spectroscopy. Nanoparticles arranged in periodic arrays produce collective resonances with a strong absorption, especially for plasmonic structures.[1–5] The collective resonances are spectrally close to the wavelength corresponding to the Rayleigh anomaly (RA) determined by the lattice spacing and the refractive index of the surrounding medium.[6] Multipole analysis can play an important role in lattice resonance analysis and the nanoparticle structure design. A series of analytical and semi-analytical multipole models have been established in the past decade. In the dipole approximation, optical responses of nanoparticles are characterized by the induced electric dipole (ED) and magnetic dipole (MD) moments in each particle.[7,8] By solving the coupled dipole equations, the effective dipole moments of particles in the lattice can be expressed in terms of the incident field, electric and magnetic polarizabilities of a single particle, and lattice sums. In subsequent works, electric quadrupoles (EQs) and magnetic quadrupoles (MQs) have been included in coupled dipole–quadrupole models for nanosphere lattices.[9–11]

Multipoles of a single spherical particle have no coupling between each other (they are eigenmodes), but ED-MQ and EQ-MD coupling effects emerge in the lattice.[11–14] Cross-multipole coupling can also be facilitated in purposely engineered structures, e.g., nanoparticles of a complex shape and their clusters, inclusion of inhomogeneities, etc. For instance, Evlyukhin *et al.*[15] have included magnetoelectric coupling in the coupled dipole model for nanoparticles of complex shapes to analyze the bianisotropic electromagnetic response and the trapped modes excited in the array.

The multipole scattering cross sections and polarizabilities for a single spherical particle can be calculated analytically through Mie theory.[16] Furthermore, generalized Mie theory can be applied to clusters of multiple particles.[17,18] Analytical models are not available for an arbitrary-shaped particle, and the multipole decomposition methods have been applied often (see, e.g., the work of Alaee *et al.*[19,20] with analytical expressions for multipole decomposition). In this technique, the derivation of expressions is based on the electric current density distribution inside the nanoparticle. The electric field radiated by the current source is then decomposed with the multipoles as the basis. Multipole decomposition is widely applied

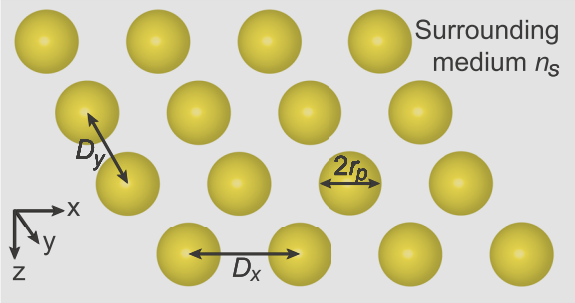

FIG. 1. Schematic of the nanosphere array in the uniform (homogeneous) surrounding medium with refractive index n_s. The two-dimensional infinite periodic arrays have the pitch D_x and D_y in the x- and y-directions, and the radius of a sphere is r_p. In this work, we study periodic arrays of both gold and silicon nanoparticles. The excitation is a linearly polarized plane wave with incidence normal to the array plane and propagating along the z-direction. We analyze both x- and y-polarized incident waves.

to a single nanoparticle or a unit cell of closely spaced nanoparticles in periodic arrays to analyze the excited multipoles.[21–24] However, few studies focused on the accuracy and the convergence of the multipole decomposition for the lattice structures and only in the case of the small distance between nanoparticles.[25,26] There has been no detailed investigation on when the wavelengths of interest are close to the lattice resonances, and strong multipole coupling exists.

In this work, we study the multipoles around the lattice resonances. We compare the multipole decomposition results with the analytic results for both plasmonic and dielectric nanostructures. This study demonstrates the applicability of multipole decomposition around lattice resonances. A few multipoles obtained from the spherical harmonics expansion can represent the accurate results, even with strong multipole coupling.

Plasmonic nanoparticles of simple shapes, such as a sphere or disk, only have strong resonances of electric multipoles. In contrast, high refractive index dielectric nanoparticles can support strong resonances of magnetic multipoles in addition to electric ones.[27,28] We study gold and silicon spherical nanoparticles in periodic arrays with strong lattice resonance excitations to examine the multipole decomposition at both the electric and magnetic resonances, as shown in Fig. 1. The gold nanoparticles can provide large electric polarizabilities, while the silicon ones have large magnetic polarizabilities. In this study, we work only with spherical particles due to the availability of analytical models. The coupled dipole–quadrupole model is used to calculate the analytical multipoles in the lattice. Section II explains the model and gives the reflection and transmission coefficients expressed by the multipole polarizabilities. Thus, we use the reflection and transmission to show the accuracy of the multipole decomposition results.

II. ANALYTICAL MODEL: DIPOLE–QUADRUPOLE COUPLING IN THE LATTICE

The coupled dipole–quadrupole model has been developed for spherical particles in periodic arrays.[11] It is used to calculate the effective polarizabilities of the excited multipoles when their lattice is illuminated normally by the plane wave. In this model, spherical particles can be considered as the point multipoles arranged into the lattice. The local electric $\mathbf{E}^{\mathrm{loc}}(\mathbf{r}_j)$ and magnetic $\mathbf{H}^{\mathrm{loc}}(\mathbf{r}_j)$ fields at each particle include the incident electromagnetic field and the additional contributions from other multipoles in the lattice, that is, electromagnetic fields induced by other particles in the array. The vectors of electric dipole moment $\mathbf{p}^j$ and magnetic dipole moment $\mathbf{m}^j$ and the tensors of the electric quadrupole moment $\hat{Q}^j$ and magnetic quadrupole moment $\hat{M}^j$ of a particle located at $\mathbf{r}_j$ can be expressed as follows:[11]

$$\mathbf{P}^j = \hat{\alpha}_p^j \boldsymbol{E}^{\mathrm{loc}}(\boldsymbol{r}_j), \tag{1}$$

$$\mathbf{m}^j = \hat{\alpha}_m^j \boldsymbol{H}^{\mathrm{loc}}(\boldsymbol{r}_j), \tag{2}$$

$$\hat{Q}^j = \frac{\hat{\alpha}_Q^j}{2}\left[\nabla \boldsymbol{E}^{\mathrm{loc}}(\boldsymbol{r}_j) + \boldsymbol{E}^{\mathrm{loc}}(\boldsymbol{r}_j)\nabla\right], \tag{3}$$

$$\hat{M}^j = \frac{\hat{\alpha}_M^j}{2}\left[\nabla \boldsymbol{H}^{\mathrm{loc}}(\boldsymbol{r}_j) + \boldsymbol{H}^{\mathrm{loc}}(\boldsymbol{r}_j)\nabla\right], \tag{4}$$

where ∇ is the nabla (or del) operator; and $\hat{\alpha}_p^j$, $\hat{\alpha}_m^j$, $\hat{\alpha}_Q^j$, and $\hat{\alpha}_M^j$ are the ED, MD, EQ, and MQ polarizability tensors of a particle located at $\mathbf{r}_j$, respectively.

Let us consider identical spherical nanoparticles in the infinite periodic rectangular array normally illuminated by an x-polarized monochromatic light wave with field components $[E_x(\mathbf{r}) = E_0 \exp(ik_s z), H_y(\mathbf{r}) = H_0 \exp(ik_s z), 0]$. In a homogeneous medium with relative permittivity ε_s, $H_0 = \sqrt{\frac{\varepsilon_0 \varepsilon_s}{\mu_0}} E_0$. As the nanoparticles are identical and $\mathbf{p}^j = \mathbf{p}$, $\mathbf{m}^j = \mathbf{m}$, $\hat{Q}^j = \hat{Q}$, and $\hat{M}^j = \hat{M}$, the dipole and quadrupole moments of the nanoparticles can be reduced to the following components: $\mathbf{p} = (p_0\hat{x} + 0\hat{y} + 0\hat{z})$, $\mathbf{m} = (0\hat{x} + m_0\hat{y} + 0\hat{z})$, $\hat{Q} = Q_0(\hat{x}\hat{z} + \hat{z}\hat{x})$, and $\hat{M} = M_0(\hat{y}\hat{z} + \hat{z}\hat{y})$, where $\hat{x}$, $\hat{y}$, and $\hat{z}$ are the unit vectors of the Cartesian coordinate system. In this case, Eqs. (1)–(4) for the general system can be simplified to the following form:

$$\begin{aligned}
p_0 &= \alpha_p E_x(\boldsymbol{r}_0) + \frac{\alpha_p}{\varepsilon_0}\left[S_{pp} p_0 + \frac{ik_0}{c} S_{pM} M_0\right],\\
m_0 &= \alpha_m H_y(\boldsymbol{r}_0) + \alpha_m\left[S_{mm} m_0 + \frac{ck_0}{i} S_{mQ} Q_0\right],\\
Q_0 &= \frac{\alpha_Q i k_s E_x(\boldsymbol{r}_0)}{2} + \frac{\alpha_Q}{2\varepsilon_0}\left[\frac{ik_0}{c} S_{Qm} m_0 + S_{QQ} Q_0\right],\\
M_0 &= \frac{\alpha_M i k_s H_y(\boldsymbol{r}_0)}{2} + \frac{\alpha_M}{2}\left[\frac{ck_0}{i} S_{Mp} p_0 + S_{MM} M_0\right],
\end{aligned} \tag{5}$$

where S_{pp}, S_{mm}, S_{QQ}, S_{MM}, S_{pM}, S_{mQ}, S_{Qm}, and S_{Mp} represent the lattice sums of the multipoles and correspond to the same-multipole (former four) or cross-multipole (latter four) coupling; see Appendix A for the detailed expressions.

Next, the effective polarizabilities can be defined as $\alpha_p^{\mathrm{eff}} = p_0/E_x$, $\alpha_m^{\mathrm{eff}} = m_0/H_y$, $\alpha_Q^{\mathrm{eff}} = 2Q_0/(ik_s E_x)$, and $\alpha_M^{\mathrm{eff}} = 2M_0/(ik_s H_y)$. For a spherical particle, the polarizabilities α_p, α_m, α_Q, and α_M can be expressed through the scattering coefficients a_1, b_1, a_2, and b_2 of Mie theory, respectively.[11] For an arbitrary particle, the polarizability tensors can be calculated through the multipole decomposition.[29]

Solving the coupled equations [Eq. (5)], one can obtain the effective polarizabilities excited in the lattice.

III. NUMERICAL MODEL

A. Multipole decomposition method

The multipole decomposition calculations are based on the induced electric polarization $\mathbf{P}(\mathbf{r}) = \varepsilon_0(\varepsilon_p - \varepsilon_s)\mathbf{E}^{\text{ins}}(\mathbf{r})$, where $\mathbf{E}^{\text{ins}}(\mathbf{r})$ is the total electric field inside the particle, ε_0 is the vacuum permittivity, and ε_p and ε_s are the relative permittivity of the particle and the surrounding medium, respectively. Multipoles are used as the basis to decompose the electromagnetic fields radiated by local polarization sources. The spherical harmonic expansions can represent the multipolar fields. All the different order multipoles form an orthonormal basis. Here, we use the Cartesian multipole representations, which are based on the spherical harmonic functions. The expressions for the multipole moments are as follows:[19,25]

$$\mathbf{p} = \int \mathbf{P} j_0(k_s r) d\boldsymbol{r} + \frac{k_s^2}{10}\int \left\{[\boldsymbol{r}\cdot\mathbf{P}]\boldsymbol{r} - \frac{1}{3}r^2\mathbf{P}\right\}\frac{15 j_2(k_s r)}{(k_s r)^2} d\boldsymbol{r}, \tag{6}$$

$$\mathbf{m} = -\frac{i\omega}{2}\int [\boldsymbol{r}\times\mathbf{P}]\frac{3 j_1(k_s r)}{k_s r} d\boldsymbol{r}, \tag{7}$$

$$\begin{aligned}\hat{Q} = &\int \left\{3(\boldsymbol{r}\otimes\mathbf{P} + \mathbf{P}\otimes\boldsymbol{r}) - 2[\boldsymbol{r}\cdot\mathbf{P}]\hat{U}\right\}\frac{3 j_1(k_s r)}{k_s r} d\boldsymbol{r} \\ &+ 6k_s^2\int \left\{5\boldsymbol{r}\otimes\boldsymbol{r}[\boldsymbol{r}\cdot\mathbf{P}] - (\boldsymbol{r}\otimes\mathbf{P} + \mathbf{P}\otimes\boldsymbol{r})r^2 - r^2[\boldsymbol{r}\cdot\mathbf{P}]\hat{U}\right\} \\ &\times \frac{j_3(k_s r)}{(k_s r)^3} d\boldsymbol{r},\end{aligned} \tag{8}$$

$$\hat{M} = \frac{\omega}{3i}\int \{[\boldsymbol{r}\times\mathbf{P}]\otimes\boldsymbol{r} + \boldsymbol{r}\otimes[\boldsymbol{r}\times\mathbf{P}]\}\frac{15 j_2(k_s r)}{(k_s r)^2} d\boldsymbol{r}, \tag{9}$$

$$\hat{O}^{(e)} = 15\int \left(\mathbf{P}\otimes\boldsymbol{r}\otimes\boldsymbol{r} + \boldsymbol{r}\otimes\mathbf{P}\otimes\boldsymbol{r} + \boldsymbol{r}\otimes\boldsymbol{r}\otimes\mathbf{P} - \hat{A}\right)\frac{j_2(k_s r)}{(k_s r)^2} d\boldsymbol{r}, \tag{10}$$

$$\begin{aligned}\hat{O}^{(m)} = &\frac{-105 i\omega}{4}\int \left\{[\boldsymbol{r}\times\mathbf{P}]\otimes\boldsymbol{r}\otimes\boldsymbol{r} + \boldsymbol{r}\otimes[\boldsymbol{r}\times\mathbf{P}]\otimes\boldsymbol{r}\right. \\ &\left. + \boldsymbol{r}\otimes\boldsymbol{r}\otimes[\boldsymbol{r}\times\mathbf{P}] - \hat{A}'\right\}\frac{j_3(k_s r)}{(k_s r)^3} d\boldsymbol{r},\end{aligned} \tag{11}$$

where k_s is the wavenumber in the surrounding medium and the integral is extended over the region where P is nonzero.[30] The notation $j_n(\rho)$ denotes the n-order spherical Bessel function, and it is defined by $j_n(\rho) = \sqrt{\pi/2\rho}J_{n+1/2}(\rho)$, where $J_n(\rho)$ is the Bessel function of the first kind. The following expressions are used:

$$A_{\beta\gamma\tau} = \delta_{\beta\gamma}V_\tau + \delta_{\beta\tau}V_\gamma + \delta_{\gamma\tau}V_\beta, \tag{12}$$

$$V = \frac{1}{5}\left[2(\boldsymbol{r}\cdot\mathbf{P})\otimes\boldsymbol{r} + r^2\mathbf{P}\right], \tag{13}$$

$$A'_{\beta\gamma\tau} = \delta_{\beta\gamma}V'_\tau + \delta_{\beta\tau}V'_\gamma + \delta_{\gamma\tau}V'_\beta, \tag{14}$$

$$V' = \frac{1}{5}r^2[\mathbf{r}\times\mathbf{p}], \tag{15}$$

where $\beta = x, y, z$, $\gamma = x, y, z$, $\tau = x, y, z$, and $\delta_{\beta\gamma}$ is the Kronecker delta.

B. Reflection and transmission coefficients represented by the multipoles

The scattered electric field $\mathbf{E}_{\boldsymbol{n}}^{sc}(\boldsymbol{r})$ in the direction $\mathbf{n}$ for a single nanoparticle can be expressed as[25,26,31]

$$\begin{aligned}\mathbf{E}_{\boldsymbol{n}}^{sc}(\boldsymbol{r}) \simeq \frac{k_0^2 e^{ik_s r}}{4\pi\varepsilon_0 r}\Bigg(&[\mathbf{n}\times(\mathbf{P}\times\mathbf{n})] + \frac{\sqrt{\varepsilon_s}}{c}[\mathbf{m}\times\mathbf{n}] + \frac{ik_s}{6}\left[\mathbf{n}\times\left(\mathbf{n}\times\hat{Q}\mathbf{n}\right)\right] \\ &+ \frac{ik_s\sqrt{\varepsilon_s}}{2c}\left[\mathbf{n}\times\left(\hat{M}\mathbf{n}\right)\right] + \frac{k_s^2}{6}\left[\mathbf{n}\times\left(\mathbf{n}\times\hat{O}^{(e)}\mathbf{nn}\right)\right] \\ &+ \frac{k_s^2\sqrt{\varepsilon_s}}{6c}\left[\mathbf{n}\times\hat{O}^{(m)}\mathbf{nn}\right]\Bigg),\end{aligned} \tag{16}$$

where c is the speed of light in the vacuum and $\mathbf{n} = \mathbf{r}/r$ is the unit vector to the scattering direction. For example, forward scattering corresponds to $\mathbf{n} = (0, 0, 1)$ and backward scattering corresponds to $\mathbf{n} = (0, 0, -1)$.

Now, let us consider a two-dimensional infinite periodic array illuminated by a normally incident and x-polarized light wave. In this case, we can derive the complex electric field reflection r and transmission t coefficients expressed with effective multipoles as follows (see, e.g., Ref. 26). These expressions correspond to the zeroth diffraction order and translate to the reflection and transmission for the wavelength larger than the diffraction limit. Here, to improve the accuracy of the transmission and reflection spectra, we extend the equations to include electric octupole (EO) and magnetic octupole (MO) terms,

$$\begin{aligned}r = \frac{ik_s}{2S_L}\Bigg(&\frac{1}{\varepsilon_0\varepsilon_s}\alpha_p^{\text{eff}} - \alpha_m^{\text{eff}} - \frac{k_0^2}{12\varepsilon_0}\alpha_Q^{\text{eff}} + \frac{k_s^2}{4}\alpha_M^{\text{eff}} \\ &+ \frac{k_s^4}{18\varepsilon_0\varepsilon_s}\alpha_{eo}^{\text{eff}} - \frac{k_s^4}{18}\alpha_{mo}^{\text{eff}}\Bigg),\end{aligned} \tag{17}$$

$$\begin{aligned}t = 1 + \frac{ik_s}{2S_L}\Bigg(&\frac{1}{\varepsilon_0\varepsilon_s}\alpha_p^{\text{eff}} + \alpha_m^{\text{eff}} + \frac{k_0^2}{12\varepsilon_0}\alpha_Q^{\text{eff}} + \frac{k_s^2}{4}\alpha_M^{\text{eff}} \\ &+ \frac{k_s^4}{18\varepsilon_0\varepsilon_s}\alpha_{eo}^{\text{eff}} + \frac{k_s^4}{18}\alpha_{mo}^{\text{eff}}\Bigg),\end{aligned} \tag{18}$$

where $S_L = D_x D_y$ is the area of a lattice unit cell, and the effective polarizabilities of ED, MD, EQ, MQ, EO, and MO are defined by $\alpha_p^{\text{eff}} = p_x/E_x$, $\alpha_m^{\text{eff}} = m_y/H_y$, $\alpha_Q^{\text{eff}} = 2Q_{xz}/(ik_s E_x)$, $\alpha_M^{\text{eff}} = 2M_{yz}/(ik_s H_y)$, $\alpha_{eo}^{\text{eff}} = -3O_{xzz}^{(e)}/(k_s^2 E_x)$, and $\alpha_{mo}^{\text{eff}} = -3O_{yzz}^{(m)}/(k_s^2 H_y)$, respectively. We show the equations written in terms of the multipole moments in Appendix A.

The reflection and transmission coefficients related to intensity are

$$R = |r|^2, \quad T = |t|^2. \tag{19}$$

For the wavelength range above the diffraction limit, when there are no higher-order reflection and transmission terms (diffraction), the

absorption coefficient can be calculated as $A = 1 - R - T$. Throughout the text, when we plot amplitudes of multipole polarizabilities, the polarizabilities are multiplied by coefficients in Eq. (17) to show their relative contribution in the reflection and transmission.

IV. RESULTS

To analyze both electric and magnetic multipole resonances, we study plasmonic (gold) and high-index dielectric (silicon) nanoparticle arrays in this section. There can be strong electric resonances in the gold particles and strong magnetic resonances in the silicon particles. We use full-wave numerical simulations[32] based on the finite element method to calculate the electric field inside particles and the corresponding transmission and reflection spectra. The multipole decomposition calculations are based on the expressions presented in Eqs. (6)–(11). For the analytics comparison, we calculate multipole polarizabilities of a single particle by Mie theory and then use the coupled dipole–quadrupole model shown in Eqs. (1)–(4) to obtain the effective multipole polarizabilities for the lattice. In addition, we also include results from a hybrid (semi-analytical) method. We apply the multipole decomposition to the simulation for a single particle with the perfectly matched layer (PML) boundary condition in all three directions. Then, we use the polarizabilities from the multipole decomposition and the coupled dipole–quadrupole model to calculate the effective multipole polarizabilities. The hybrid method is handy when we deal with nanoparticles of a non-spherical shape.

A. Gold (plasmonic) nanoparticles and their lattices

Let us consider the plasmonic metasurfaces of spherical gold nanoparticle arrays embedded in a homogeneous environment with refractive index $n_s = 1.47$, as shown in Fig. 1. The two-dimensional infinite periodic arrays have the spacings $D_x = 510$ nm and $D_y = 250$ nm, and the gold spheres have $r_p = 100$ nm. Here, the relative permittivities of the particle and the surrounding medium are $\varepsilon_p = \varepsilon_{\mathrm{Au}}$ and $\varepsilon_s = n_s^2$, respectively. The gold permittivity is fitted by $\varepsilon_{\mathrm{Au}} = \varepsilon_\infty - \omega_p^2/(\omega^2 + i\gamma\omega)$, where $\varepsilon_\infty = 2.4023$, $\omega_p = 1.2122 \times 10^{36}$ rad/s, and $\gamma = 3.9941 \times 10^{14}$ rad/s.

The first step is to compare the analytical results with numerical ones for a single (isolated) nanoparticle in an infinite uniform environment. Multipole analysis of the single spherical gold particle with radius $r_p = 100$ nm embedded in a homogeneous environment with refractive index $n_s = 1.47$ is shown in Fig. 2. The plot shows absolute values of the multipole polarizabilities calculated through both Mie theory and the multipole decomposition. We consider a sphere illuminated by an x-polarized plane wave that propagates in the z-direction and then apply the multipole decomposition. Figure 2 shows that the results are in good agreement with Mie theory. Then, we apply the multipole analysis to the periodic metasurfaces consisting of the regular lattice of the same nanoparticles. Figure 3 shows the transmission and reflection spectra for the metasurfaces under the illumination of the x-polarized plane wave. The transmission and reflection spectra can be computed by the multipole moments using Eqs. (B1), (B2), and (19). Applying the multipole decomposition to the simulation of the nanoparticle arrays, we obtain the effective multipole moments for each particle inside the lattice (denoted as "Multipole" in Fig. 3). Here, we include ED, MD, EQ, MQ, EO, and MO terms. Following the common approach, to reduce the unnecessary high-order multipoles moments, we choose the center of the nanoparticle as the coordinate origin of the multipole decomposition. As a comparison, we also show the results using the single particle multipole decomposition and the electromagnetic dipole–quadrupole coupling model (denoted as "Hybrid"

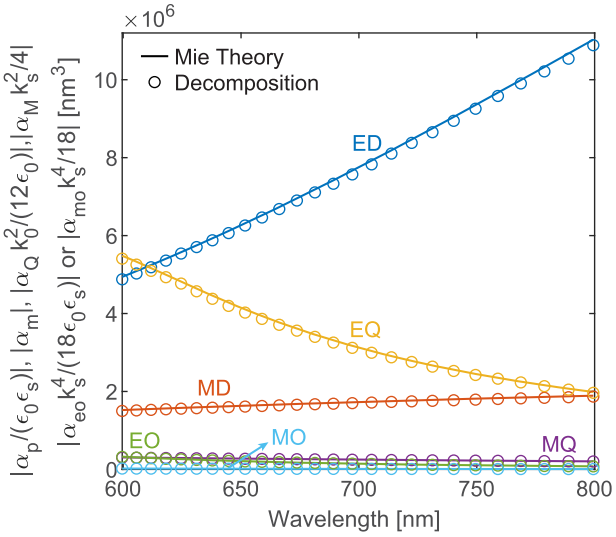

FIG. 2. Single gold nanosphere multipoles: Absolute values of the multipole polarizabilities [multiplied by corresponding coefficients; see Eq. (17)]. The sphere radius is $r_p = 100$ nm, and it is embedded in a homogeneous environment with refractive index $n_s = 1.47$. The plot shows the comparison between Mie theory and the multipole decomposition calculation based on numerical simulations.

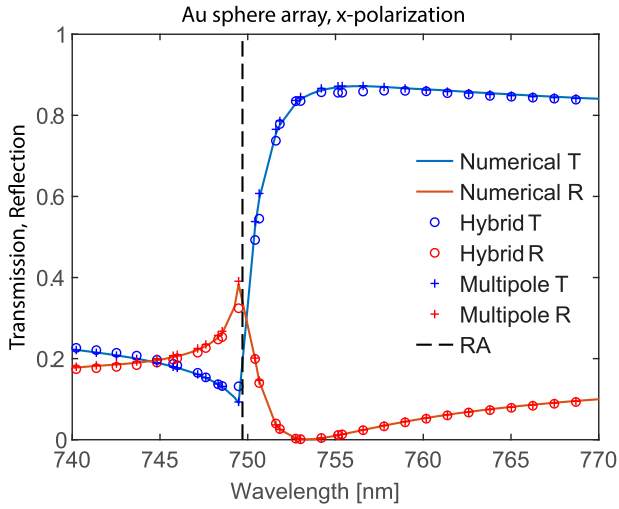

FIG. 3. Spectra of the transmission T and reflection R of the gold nanosphere array with the x-polarized incident electric field. The lattice periods are $D_x = 510$ nm and $D_y = 250$ nm, and the gold spheres have $r_p = 100$ nm. The homogeneous environment has refractive index $n_s = 1.47$. The "RA" line denotes the wavelength of the Rayleigh anomaly.

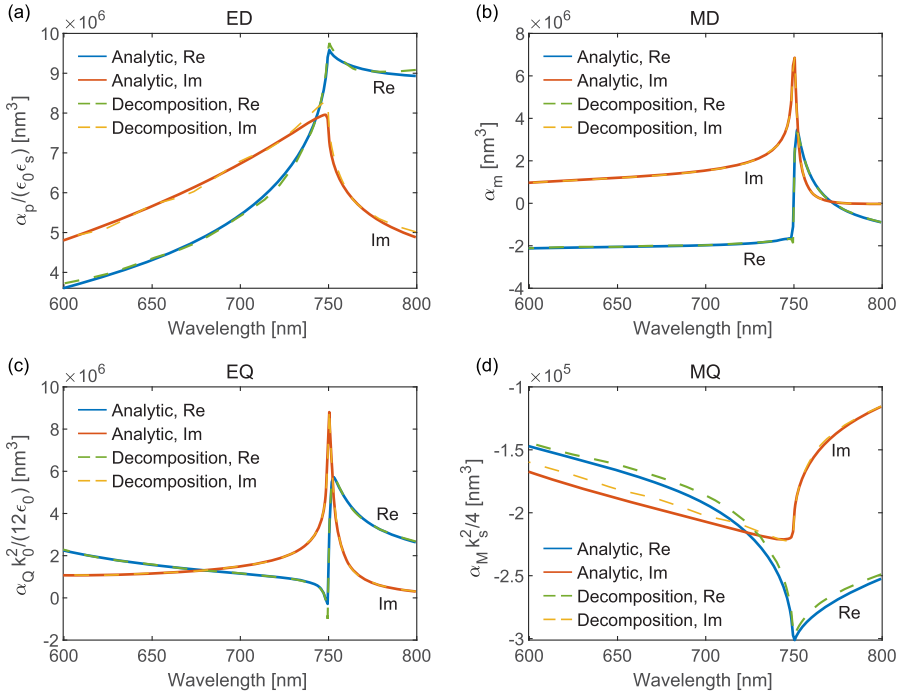

FIG. 4. Comparison of the multipole effective polarizabilities: (a) ED, (b) MD, (c) EQ, and (d) MQ for the gold nanosphere array. The structure is the same as in Fig. 3. The light is *x*-polarized; the homogeneous environment has refractive index $n_s = 1.47$; the lattice periods are $D_x = 510$ nm and $D_y = 250$ nm; and the gold spheres have $r_p = 100$ nm.

in Fig. 3). The coupling of ED-MQ and EQ-MD is taken into account in the model. Both of the methods show excellent agreement with the numerical results with full-wave simulations.

Figure 4 shows the effective polarizabilities of each multipole. The multipole decomposition results agree well with those from the analytical model. The sharp lattice resonance in the linear spectra is caused by the resonances of EQ and MD multipoles. It can be represented by a few low-order multipole moments.

Finally, we analyze the case of the ED lattice resonance. Figure 5 shows the transmission and reflection spectra for the metasurfaces under the illumination of the *y*-polarized plane wave. The broad ED resonance is excited around $\lambda = 950$ nm. The multipole decomposition for the lattice simulation is again in good agreement with the numerical results. However, there is a little mismatch with the results obtained with the analytical model. The likely origin of the mismatch is a considerable value of the EO multipole, which is not included in the analytical model. The EO moment is larger compared with previous case and potentially may have a coupling component to ED.

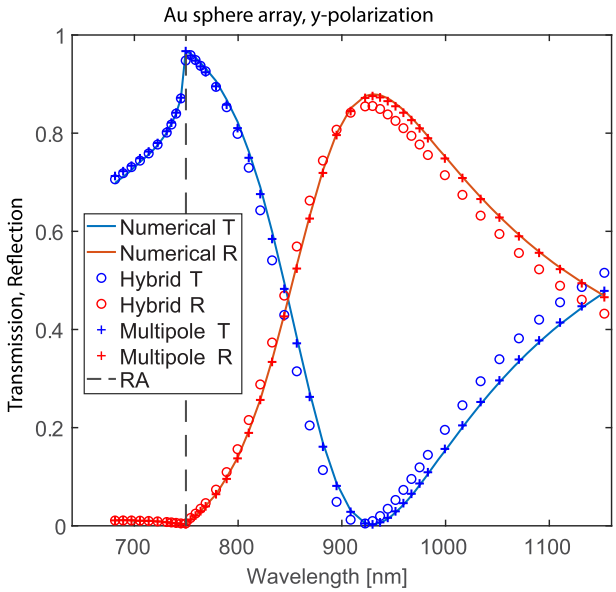

FIG. 5. Spectra of the transmission *T* and reflection *R* of the gold nanosphere array with the *y*-polarized incident electric field. The lattice periods are $D_x = 510$ nm and $D_y = 250$ nm, and the gold spheres have $r_p = 100$ nm. The homogeneous environment has refractive index $n_s = 1.47$. The "RA" line denotes the wavelength of the Rayleigh anomaly.

B. Silicon nanoparticles and their lattices

Excitation of strong magnetic resonances in plasmonic nanoparticles requires a purposely engineered shape with the combination of metal and dielectric materials. At the same time, the spherical nanoparticles made of a high-index dielectric material can support not only strong electric but also magnetic resonances because of the electric field penetration inside the particle. These nanoparticles give us an opportunity to analyze the lattice resonance with strong magnetic multipoles and the analytical model reduced for the case of spherical particles. Let us consider the silicon spherical-nanoparticle array embedded in the air ($n_s = 1$). The two-dimensional infinite periodic array has the spacings $D_x = 780$ nm and $D_y = 590$ nm, and the silicon spheres have radius $r_p = 100$ nm. In this case, the relative permittivities of the particle and

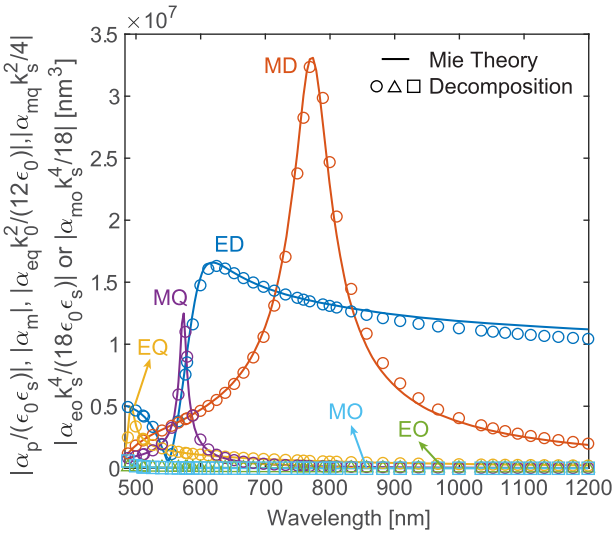

FIG. 6. Absolute values of the multipole polarizabilities for a single silicon sphere with radius $r_p = 100$ nm in the air ($n_s = 1$). The plot shows the comparison between Mie theory and the multipole decomposition calculation based on numerical simulations.

the surrounding medium are $\varepsilon_p = \varepsilon_{\mathrm{Si}}$ and $\varepsilon_s = n_s^2 = 1$, respectively. Silicon permittivity $\varepsilon_{\mathrm{Si}}$ is taken from Ref. 33.

Figure 6 shows absolute values of the multipole polarizabilities for a single silicon sphere in the air. There is a strong MD resonance around $\lambda = 773$ nm for a single silicon sphere. We choose the lattice spacing $D_x = 780$ nm to make the wavelength of the Rayleigh anomaly close to the MD resonance of the single particle. Figure 7

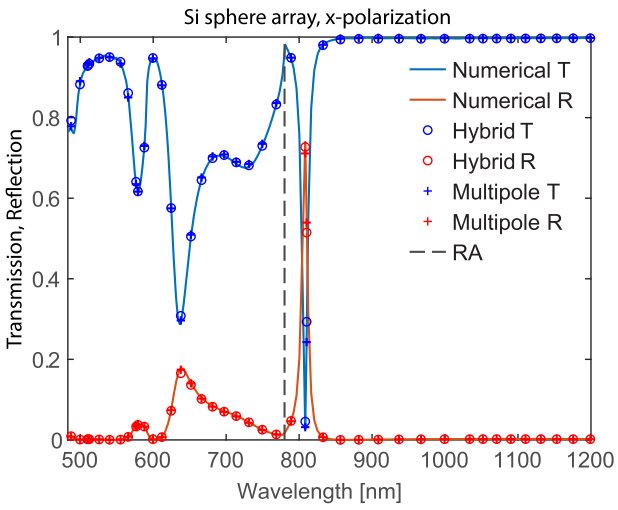

FIG. 7. Spectra of the transmission T and reflection R of the silicon nanosphere array with the x-polarized incident electric field. The lattice periods are $D_x = 780$ nm and $D_y = 590$ nm, and the silicon spheres have $r_p = 100$ nm. The surrounding medium is air ($n_s = 1$). The "RA" line denotes the wavelength of the Rayleigh anomaly.

shows the transmission and reflection spectra for the metasurfaces under the illumination of the x-polarized plane wave. The multipole decomposition results agree well with the numerical results, including the strong MD lattice resonance at $\lambda = 810$ nm. This shows the validity of the multipole decomposition method around the wavelength of a strong magnetic lattice resonance.

V. NUMERICAL CHALLENGES AND DISCUSSIONS

This section highlights some aspects of the numerical simulations and the challenges overcome in the investigation. One should be particularly careful when setting up the parameters of the numerical simulations for accurate results. When a lattice resonance is close to the Rayleigh anomaly in the spectrum, near fields can extend to long distances in the beam propagation direction. Although it is the wavelength above the diffraction limit and the first diffraction order experiences a cut-off, the tails of the first diffraction order still contribute considerably. Thus, large simulation domains in the z-direction are needed for lattice simulations. Large simulation domains are also required for accurate simulations for the wavelength range in the proximity to the next diffraction order. In addition, the multipole decomposition method shown in Eqs. (6)–(11) works in the frequency domain. If the numerical simulation is solved by a time-domain method, one needs to transform the electric field to the frequency domain for the multipole decomposition.

In the course of numerical simulations, we find that the numerical dispersion in the lattice simulation may cause a phase shift of the multipole moments (especially for ED) in the multipole decomposition and may lead to errors in the transmission and reflection spectra. There should be enough mesh nodes in the computation domain outside the particles to obtain an accurate electric field inside the particles. We observed that this issue does not affect the absolute values of multipole moments, and it might be challenging to find out the origin of result inconsistency if we only compare the amplitudes in simulations and analytic calculations. This phase information can be confirmed by calculating the transmission and reflection based on the obtained multipole polarizabilities.

It should also be noted that we choose the center of the nanoparticle as the coordinate origin of the multipole decomposition. It reduces the unnecessary high-order multipole moment contribution and allows us to use a few multipoles to represent the electromagnetic field scattered by the structure accurately.

The multipole decomposition method can be applied to arbitrarily shaped particles. We choose the spherical particle arrays to be able to compare with the analytical results and thus have a reference for accuracy. Calculation of cross-sections of the multiple-sphere system can be performed by generalizing Mie theory.[17,18] The total electric field from the system (incident, internal, and scattered electric field) can be expressed as the vector spherical harmonics expansions by applying the corresponding boundary conditions. For particles arranged in arrays, including one- and two-dimensional cases with a short or long distance, the multipole coupling can be approximated using similar ways with vector spherical harmonics and matching boundary conditions. The general goal is to reduce computational resources and obtain higher accuracy results with fewer multipoles accounted. A recent example of such research is an analysis of multipole-decomposition approaches for directional light

scattering in a finite spatial region and demonstrating a much better convergence of results with the long-wavelength approximation than with the exact multipoles obtained from the spherical harmonics expansion even in the case of the relatively large scatterer.[25] To express the electromagnetic fields with a few multipoles and high accuracy, we choose to employ the coupled dipole–quadrupole model, which has been developed for spherical particles in periodic arrays.[11] The multipole decomposition under consideration can be applied to particles of various shapes, and therefore an important tool in the investigation of multipole systems.

VI. CONCLUSION

This work aimed at examining the multipole decomposition results around the lattice resonances. The spectra of effective multipoles excited in the periodic nanoparticle array close to the Rayleigh anomaly are very different from those for the single-particle. The lattice structure facilitates strong resonances because of the same-multipole and cross-multipole couplings. Using the multipole decomposition method, we showed that we could obtain accurate reflection and transmission spectra even at sharp lattice resonances. These findings indicate that we can use a few low-order multipoles to describe the scattering properties of the lattice structure. We also report on numerical challenges that were overcome in modeling the nanoparticle lattices. The numerical simulation should be set up carefully to reduce the numerical dispersion in the domain with a long wave-propagation distance. This study helps deepen the understanding of the multipole analysis for the lattice arrays and will be helpful in the theoretical development and novel metasurface design.

ACKNOWLEDGMENTS

A.H. and J.V.M. acknowledge the support from the Air Force Office of Scientific Research under Grant No. FA9550-19-1-0032 and a DURIP instrumentation under Grant No. FA9550-18-1-0368. V.E.B. acknowledges the support from the University of New Mexico Research Allocations Committee (Award No. RAC 2022) and WeR1: Investing in Faculty Success Program for the computational resources.

AUTHOR DECLARATIONS

Conflict of Interest

All authors declare that they have no conflicts of interest.

DATA AVAILABILITY

The data that support the findings of this study are available within the article and are available from the corresponding author upon reasonable request.

APPENDIX A: EXPRESSIONS FOR THE LATTICE SUM IN THE COUPLED DIPOLE–QUADRUPOLE MODEL

The expressions for the lattice sum S_{pp}, S_{mm}, S_{QQ}, S_{MM}, S_{pM}, S_{mQ}, S_{Qm}, and S_{Mp} are[11]

$$S_{pp} \equiv k_0^2 \sum_{l\neq 0} G_{xx}^p(0,\boldsymbol{r}_l) = \frac{k_0^2}{4\pi}\sum_{l\neq 0}\frac{e^{ik_s r_l}}{r_l}\left(1+\frac{i}{k_s r_l}-\frac{1}{k_s^2 r_l^2}-\frac{x_l^2}{r_l^2}-\frac{i3x_l^2}{k_s r_l^3}+\frac{3x_l^2}{k_s^2 r_l^4}\right), \tag{A1}$$

$$S_{mm} \equiv k_s^2 \sum_{l\neq 0} G_{yy}^p(0,\boldsymbol{r}_l) = \frac{k_s^2}{4\pi}\sum_{l\neq 0}\frac{e^{ik_s r_l}}{r_l}\left(1+\frac{i}{k_s r_l}-\frac{1}{k_s^2 r_l^2}-\frac{y_l^2}{r_l^2}-\frac{i3y_l^2}{k_s r_l^3}+\frac{3y_l^2}{k_s^2 r_l^4}\right), \tag{A2}$$

$$S_{QQ} = \frac{k_0^2}{6}\frac{ik_s}{4\pi}\sum_{l\neq 0}\frac{e^{ik_s r_l}}{r_l^2}\left(-2-i\frac{6+k_s^2x_l^2}{k_s r_l}+\frac{12+7k_s^2x_l^2}{k_s^2 r_l^2} + i\frac{12+27k_s^2x_l^2}{k_s^3 r_l^3}-\frac{60x_l^2}{k_s^2 r_l^4}-\frac{i60x_l^2}{k_s^3 r_l^5}\right), \tag{A3}$$

$$S_{MM} = \frac{k_0^2\varepsilon_S}{2}\frac{ik_s}{4\pi}\sum_{l\neq 0}\frac{e^{ik_s r_l}}{r_l^2}\left(-2-i\frac{6+k_s^2y_l^2}{k_s r_l}+\frac{12+7k_s^2y_l^2}{k_s^2 r_l^2} + i\frac{12+27k_s^2y_l^2}{k_s^3 r_l^3}-\frac{60y_l^2}{k_s^2 r_l^4}-\frac{i60y_l^2}{k_s^3 r_l^5}\right), \tag{A4}$$

$$S_{mQ} \equiv \frac{1}{Q_0}\sum_{l\neq 0}\left[\boldsymbol{q}_{0l}\times\left(\hat{Q}^l\boldsymbol{n}_{l0}\right)\right]_y = \frac{1}{6}\frac{k_s^2}{4\pi}\sum_{l\neq 0}\frac{x_l^2 e^{ik_s r_l}}{r_l^3}\left(-1-\frac{3i}{k_s r_l}+\frac{3}{k_s^2 r_l^2}\right), \tag{A5}$$

$$S_{Qm} \equiv \frac{1}{m_0}\sum_{l\neq 0}\left[\nabla_0\left[\mathbf{g}_{0l}\times\mathbf{m}^l\right]+\left[\mathbf{g}_{0l}\times\mathbf{m}^l\right]\nabla_0\right]_{xz} = 6S_{mQ} = \frac{k_s^2}{4\pi}\sum_{l\neq 0}\frac{x_l^2 e^{ik_s r_l}}{r_l^3}\left(-1-\frac{3i}{k_s r_l}+\frac{3}{k_s^2 r_l^2}\right), \tag{A6}$$

$$S_{pM} \equiv \frac{1}{M_0}\sum_{l\neq 0}\left[\boldsymbol{q}_{0l}\times\left(\hat{M}^l\boldsymbol{n}_{l0}\right)\right]_x = \frac{-k_s^2}{8\pi}\sum_{l\neq 0}\frac{y_l^2 e^{ik_s r_l}}{r_l^3}\left(-1-\frac{3i}{k_s r_l}+\frac{3}{k_s^2 r_l^2}\right), \tag{A7}$$

$$S_{Mp} \equiv \frac{1}{p_0}\sum_{l\neq 0}\left[\nabla_0\left[\mathbf{g}_{0l}\times\mathbf{p}^l\right]+\left[\mathbf{g}_{0l}\times\mathbf{p}^l\right]\nabla_0\right]_{yz} = 2S_{pM} = \frac{-k_s^2}{4\pi}\sum_{l\neq 0}\frac{y_l^2 e^{ik_s r_l}}{r_l^3}\left(-1-\frac{3i}{k_s r_l}+\frac{3}{k_s^2 r_l^2}\right). \tag{A8}$$

The general equations for the coupled dipole–quadrupole model are as following:[11]

$$\mathbf{p}^j = \hat{\alpha}_p^j\boldsymbol{E}_0(\boldsymbol{r}_j) + \hat{\alpha}_p^j\frac{k_0^2}{\varepsilon_0}\sum_{l\neq j}^{N}\left\{\hat{G}_{jl}^p\mathbf{p}^l+\frac{i}{ck_0}\left[\mathbf{g}_{jl}\times\mathbf{m}^l\right] + \hat{G}_{jl}^Q\left(\hat{Q}^l\boldsymbol{n}_{lj}\right)+\frac{3i}{ck_0}\left[\boldsymbol{q}_{jl}\times\left(\hat{M}^l\boldsymbol{n}_{lj}\right)\right]\right\}, \tag{A9}$$

$$\mathbf{m}^j = \hat{\alpha}_m^j \boldsymbol{H}_0(\boldsymbol{r}_j) + \hat{\alpha}_m^j k_0^2 \sum_{l\neq j}^{N} \left\{ \frac{c}{ik_0}\left[\mathbf{g}_{jl}\times\mathbf{p}^l\right] + \varepsilon_s \hat{G}_{jl}^p \mathbf{m}^l + \frac{c}{ik_0}\left[\boldsymbol{q}_{jl}\times\left(\hat{Q}^l\boldsymbol{n}_{lj}\right)\right] + 3\varepsilon_s \hat{G}_{jl}^Q\left(\hat{M}^l\boldsymbol{n}_{lj}\right)\right\}, \tag{A10}$$

$$\begin{aligned}\hat{Q}^j = {}& \frac{\hat{\alpha}_Q^j}{2}\left[\nabla \boldsymbol{E}_0(\boldsymbol{r}_j) + \boldsymbol{E}_0(\boldsymbol{r}_j)\nabla\right] \\ & + \frac{\hat{\alpha}_Q^j k_0^2}{2\varepsilon_0}\sum_{l\neq j}^{N}\left\{\left[\nabla_j\left(\hat{G}_{jl}^p\mathbf{p}^l\right) + \left(\hat{G}_{jl}^p\mathbf{p}^l\right)\nabla_j\right]\right. \\ & + \frac{i}{ck_0}\left(\nabla_j\left[\mathbf{g}_{jl}\times\mathbf{m}^l\right] + \left[\mathbf{g}_{jl}\times\mathbf{m}^l\right]\nabla_j\right) \\ & + \left\{\nabla_j\left[\hat{G}_{jl}^Q\left(\hat{Q}^l\boldsymbol{n}_{lj}\right)\right] + \left[\hat{G}_{jl}^Q\left(\hat{Q}^l\boldsymbol{n}_{lj}\right)\right]\nabla_j\right\} \\ & \left. + \frac{3i}{ck_0}\left\{\nabla_j\left[\boldsymbol{q}_{jl}\times\left(\hat{M}^l\boldsymbol{n}_{lj}\right)\right] + \left[\boldsymbol{q}_{jl}\times\left(\hat{M}^l\boldsymbol{n}_{lj}\right)\right]\nabla_j\right\}\right\},\end{aligned} \tag{A11}$$

$$\begin{aligned}\hat{M}^j = {}& \frac{\hat{\alpha}_M^j}{2}\left[\nabla \boldsymbol{H}_0(\boldsymbol{r}_j) + \boldsymbol{H}_0(\boldsymbol{r}_j)\nabla\right] \\ & + \frac{\hat{\alpha}_M^j k_0^2}{2}\sum_{l\neq j}^{N}\left\{\frac{c}{ik_0}\left(\nabla_j\left[\mathbf{g}_{lj}\times\mathbf{p}^l\right] + \left[\mathbf{g}_{lj}\times\mathbf{p}^l\right]\nabla_j\right)\right. \\ & + \varepsilon_s\left[\nabla_j\left(\hat{G}_{jl}^p\mathbf{m}^l\right) + \left(\hat{G}_{jl}^p\mathbf{m}^l\right)\nabla_j\right] \\ & + \frac{c}{ik_0}\left\{\nabla_j\left[\boldsymbol{q}_{jl}\times\left(\hat{Q}^l\boldsymbol{n}_{lj}\right)\right] + \left[\boldsymbol{q}_{jl}\times\left(\hat{Q}^l\boldsymbol{n}_{lj}\right)\right]\nabla_j\right\} \\ & \left. + 3\varepsilon_s\left\{\nabla_j\left[\hat{G}_{jl}^Q\left(\hat{M}^l\boldsymbol{n}_{lj}\right)\right] + \left[\hat{G}_{jl}^Q\left(\hat{M}^l\boldsymbol{n}_{lj}\right)\right]\nabla_j\right\}\right\},\end{aligned} \tag{A12}$$

where $\hat{G}$ denotes the corresponding field propagator of each multipole (see the Refs. 9 and 11).

APPENDIX B: REFLECTION AND TRANSMISSION COEFFICIENTS REPRESENTED BY THE MULTIPOLE MOMENTS

The general expressions for the reflection and transmission coefficients represented by the multipole moments in the case of x-polarization,

$$r = \frac{ik_s}{E_0 2S_L\varepsilon_0\varepsilon_s}\left(p_x - \frac{\sqrt{\varepsilon_s}}{c}m_y + \frac{ik_s}{6}Q_{xz} - \frac{ik_s\sqrt{\varepsilon_s}}{2c}M_{yz} - \frac{k_s^2}{6}O_{xzz}^{(e)} + \frac{k_s^2\sqrt{\varepsilon_s}}{6c}O_{yzz}^{(m)}\right), \tag{B1}$$

$$t = 1 + \frac{ik_s}{E_0 2S_L\varepsilon_0\varepsilon_s}\left(p_x + \frac{\sqrt{\varepsilon_s}}{c}m_y - \frac{ik_s}{6}Q_{xz} - \frac{ik_s\sqrt{\varepsilon_s}}{2c}M_{yz} - \frac{k_s^2}{6}O_{xzz}^{(e)} - \frac{k_s^2\sqrt{\varepsilon_s}}{6c}O_{yzz}^{(m)}\right), \tag{B2}$$

and in the case of y-polarization,

$$r = \frac{ik_s}{E_0 2S_L\varepsilon_0\varepsilon_s}\left(p_y + \frac{\sqrt{\varepsilon_s}}{c}m_x + \frac{ik_s}{6}Q_{yz} + \frac{ik_s\sqrt{\varepsilon_s}}{2c}M_{xz} - \frac{k_s^2}{6}O_{yzz}^{(e)} - \frac{k_s^2\sqrt{\varepsilon_s}}{6c}O_{xzz}^{(m)}\right), \tag{B3}$$

$$t = 1 + \frac{ik_s}{E_0 2S_L\varepsilon_0\varepsilon_s}\left(p_y - \frac{\sqrt{\varepsilon_s}}{c}m_x - \frac{ik_s}{6}Q_{yz} + \frac{ik_s\sqrt{\varepsilon_s}}{2c}M_{xz} - \frac{k_s^2}{6}O_{yzz}^{(e)} + \frac{k_s^2\sqrt{\varepsilon_s}}{6c}O_{xzz}^{(m)}\right). \tag{B4}$$

REFERENCES

[1] S. Zou, N. Janel, and G. C. Schatz, "Silver nanoparticle array structures that produce remarkably narrow plasmon lineshapes," J. Chem. Phys. **120**, 10871–10875 (2004).
[2] V. A. Markel, "Divergence of dipole sums and the nature of non-Lorentzian exponentially narrow resonances in one-dimensional periodic arrays of nanospheres," J. Phys. B: At., Mol. Opt. Phys. **38**, L115 (2005).
[3] B. Auguié and W. L. Barnes, "Collective resonances in gold nanoparticle arrays," Phys. Rev. Lett. **101**, 143902 (2008).
[4] P. Offermans, M. C. Schaafsma, S. R. K. Rodriguez, Y. Zhang, M. Crego-Calama, S. H. Brongersma, and J. Gómez Rivas, "Universal scaling of the figure of merit of plasmonic sensors," ACS Nano **5**, 5151–5157 (2011).
[5] W. Wang, M. Ramezani, A. I. Väkeväinen, P. Törmä, J. G. Rivas, and T. W. Odom, "The rich photonic world of plasmonic nanoparticle arrays," Mater. Today **21**, 303–314 (2018).
[6] V. G. Kravets, A. V. Kabashin, W. L. Barnes, and A. N. Grigorenko, "Plasmonic surface lattice resonances: A review of properties and applications," Chem. Rev. **118**, 5912–5951 (2018).
[7] S. Tretyakov, *Analytical Modeling in Applied Electromagnetics* (Artech House, 2003).
[8] A. B. Evlyukhin, C. Reinhardt, A. Seidel, B. S. Luk'yanchuk, and B. N. Chichkov, "Optical response features of Si-nanoparticle arrays," Phys. Rev. B **82**, 045404 (2010).
[9] A. B. Evlyukhin, C. Reinhardt, U. Zywietz, and B. N. Chichkov, "Collective resonances in metal nanoparticle arrays with dipole-quadrupole interactions," Phys. Rev. B **85**, 245411 (2012).
[10] V. E. Babicheva and A. B. Evlyukhin, "Metasurfaces with electric quadrupole and magnetic dipole resonant coupling," ACS Photonics **5**, 2022–2033 (2018).
[11] V. E. Babicheva and A. B. Evlyukhin, "Analytical model of resonant electromagnetic dipole-quadrupole coupling in nanoparticle arrays," Phys. Rev. B **99**, 195444 (2019).
[12] S. D. Swiecicki and J. E. Sipe, "Surface-lattice resonances in two-dimensional arrays of spheres: Multipolar interactions and a mode analysis," Phys. Rev. B **95**, 195406 (2017).
[13] S. D. Swiecicki and J. E. Sipe, "Periodic green functions for 2D magneto-electric quadrupolar arrays: Explicitly satisfying the optical theorem," J. Opt. **19**, 095006 (2017).
[14] A. Han, C. Dineen, V. E. Babicheva, and J. V. Moloney, "Second harmonic generation in metasurfaces with multipole resonant coupling," Nanophotonics **9**, 3545–3556 (2020).
[15] A. B. Evlyukhin, V. R. Tuz, V. S. Volkov, and B. N. Chichkov, "Bianisotropy for light trapping in all-dielectric metasurfaces," Phys. Rev. B **101**, 205415 (2020).
[16] C. F. Bohren and D. R. Huffman, *Absorption and Scattering of Light by Small Particles* (John Wiley & Sons, 2008).
[17] D. W. Mackowski, "Calculation of total cross sections of multiple-sphere clusters," J. Opt. Soc. Am. A **11**, 2851–2861 (1994).
[18] Y.-l. Xu, "Electromagnetic scattering by an aggregate of spheres," Appl. Opt. **34**, 4573–4588 (1995).
[19] R. Alaee, C. Rockstuhl, and I. Fernandez-Corbaton, "An electromagnetic multipole expansion beyond the long-wavelength approximation," Opt. Commun. **407**, 17–21 (2018).

[20]R. Alaee, C. Rockstuhl, and I. Fernandez-Corbaton, "Exact multipolar decompositions with applications in nanophotonics," Adv. Opt. Mater. **7**, 1800783 (2019).
[21]A. B. Evlyukhin, C. Reinhardt, and B. N. Chichkov, "Multipole light scattering by nonspherical nanoparticles in the discrete dipole approximation," Phys. Rev. B **84**, 235429 (2011).
[22]A. E. Miroshnichenko, A. B. Evlyukhin, Y. F. Yu, R. M. Bakker, A. Chipouline, A. I. Kuznetsov, B. Luk'yanchuk, B. N. Chichkov, and Y. S. Kivshar, "Nonradiating anapole modes in dielectric nanoparticles," Nat. Commun. **6**, 8069 (2015).
[23]R. Colom, R. McPhedran, B. Stout, and N. Bonod, "Modal expansion of the scattered field: Causality, nondivergence, and nonresonant contribution," Phys. Rev. B **98**, 085418 (2018).
[24]R. Colom, R. McPhedran, B. Stout, and N. Bonod, "Modal analysis of anapoles, internal fields, and Fano resonances in dielectric particles," J. Opt. Soc. Am. B **36**, 2052–2061 (2019).
[25]A. B. Evlyukhin and B. N. Chichkov, "Multipole decompositions for directional light scattering," Phys. Rev. B **100**, 125415 (2019).
[26]P. D. Terekhov, V. E. Babicheva, K. V. Baryshnikova, A. S. Shalin, A. Karabchevsky, and A. B. Evlyukhin, "Multipole analysis of dielectric metasurfaces composed of nonspherical nanoparticles and lattice invisibility effect," Phys. Rev. B **99**, 045424 (2019).
[27]I. Staude, A. E. Miroshnichenko, M. Decker, N. T. Fofang, S. Liu, E. Gonzales, J. Dominguez, T. S. Luk, D. N. Neshev, I. Brener *et al.*, "Tailoring directional scattering through magnetic and electric resonances in subwavelength silicon nanodisks," ACS Nano **7**, 7824–7832 (2013).
[28]M. Decker, I. Staude, M. Falkner, J. Dominguez, D. N. Neshev, I. Brener, T. Pertsch, and Y. S. Kivshar, "High-efficiency dielectric Huygens' surfaces," Adv. Opt. Mater. **3**, 813–820 (2015).
[29]M. Yazdi and N. Komjani, "Polarizability calculation of arbitrary individual scatterers, scatterers in arrays, and substrated scatterers," J. Opt. Soc. Am. B **33**, 491–500 (2016).
[30]J. D. Jackson, *Classical Electrodynamics* (Wiley, New York, 1999).
[31]A. B. Evlyukhin, C. Reinhardt, E. Evlyukhin, and B. N. Chichkov, "Multipole analysis of light scattering by arbitrary-shaped nanoparticles on a plane surface," J. Opt. Soc. Am. B **30**, 2589–2598 (2013).
[32]See https://www.cst.com for CST Studio Suite.
[33]E. D. Palik, *Handbook of Optical Constants of Solids* (Academic Press, 1998).